Chemical Engineering Journal 481 (2024) 148614

Contents lists available at ScienceDirect

Chemical Engineering Journal

journal homepage: www.elsevier.com/locate/cej

Black phosphorus nanosheets inhibit glioblastoma cell migration and invasion through modulation of *WNT/β-catenin* and *NOTCH* signaling pathways

Yue Xiong [a], Chao He [a,b], Xun Lin [a], Ke Cheng [a], Fumei He [a], Jingxin Zhao [a], Mengjie Yang [a], Hong Gao [a], Fangjie He [a], Xiaopei Zhang [c], Zeqi Liu [a], Gan Liu [a,*], Wenbin Deng [a,*]

[a] School of Pharmaceutical Sciences (Shenzhen), Shenzhen Campus of Sun Yat-sen University, Shenzhen, 518107, China
[b] Institute of Biomedical Health Technology and Engineering, Shenzhen Bay Laboratory, Shenzhen, 518132, China
[c] Division of Pharmacoengineering and Molecular Pharmaceutics, Eshelman School of Pharmacy, The University of North Carolina at Chapel Hill, Chapel Hill, NC 27588, USA

ARTICLE INFO

Keywords:
Black phosphorus nanosheet
Glioblastoma
Migration and invasion
WNT/β-catenin signaling pathway
GSK-3β
CSNK2A2

ABSTRACT

Black phosphorus nanosheet (BPNS) has recently demonstrated intrinsic anti-tumor bioactivity, but its underlying molecular mechanism remains unclear, limiting its potential applications in biomedicine. In this study, we investigated the impact of BPNS on glioblastoma cells and observed a significant dose-dependent inhibition of invasion and migration. RNA sequencing analysis revealed downregulation of genes associated with the *WNT/β-catenin* and *NOTCH* signaling pathways, both linked to invasion and migration. Mechanistically, BPNS directly binds to CSNK2A2, reducing its kinase activity, which indirectly enhances GSK-3β kinase activity. As a result, GSK-3β increases the phosphorylation level of β-catenin, leading to its degradation and subsequent inhibition of downstream molecules in the *WNT/β-catenin* signaling pathway. Our study uncovers the inherent biological activity of BPNS in hindering glioblastoma invasion and migration and sheds light on the molecular mechanisms, offering new directions for the nanomaterial's biomedical applications.

1. Introduction

Black phosphorus nanosheet (BPNS) has gained significant attention in recent years due to its unique properties, such as a large specific surface area, excellent biocompatibility, and promising photothermal characteristics [1–3]. These attributes have enabled its application in various fields, including photodynamic and photoacoustic therapy [4–7], drug delivery [8], bioimaging [9], and multimodal cancer theranostics [10–12]. Moreover, researchers have discovered inherent biological activities of BPNS, such as promoting inflammatory response [13], causing cell cycle arrest and blocking autophagy [14]. These discoveries have opened new avenues for potential biomedical and cancer therapy applications [15]. A previous study performed by Yu et al. demonstrated that BPNS selectively inhibits tumor cell proliferation through cell cycle arrest by binding with PLK1 kinase and destabilizing the mitotic centrosome [16]. These findings collectively suggest that BPNS may hold promise as a novel approach for cancer therapy based on its intrinsic antitumor capabilities.

Glioblastoma (GBM) represents the most malignant and aggressive form of glioma, accounting for 46.1 % of primary brain malignant tumors [17]. The high rates of migration and invasion in malignant GBM make it challenging to treat effectively[18,19]. Presently, the limited drugs available for GBM treatment, like temozolomide, face several obstacles, including the natural blockade of the blood–brain barrier (BBB), invasiveness of glioblastoma cells, tumor heterogeneity, and drug resistance[20]. BPNS-based agents have shown potential in treating neurodegenerative diseases due to their negative surface charge, modifiability, and photothermal properties, which enhance BBB permeability and enable successful drug delivery[21–27]. Given BPNS's ability to counteract tumors and its capability to cross the BBB under near-infrared (NIR) light, we hypothesize that BPNS could be a promising therapeutic candidate against GBM.

In this study, we investigated how BPNS inhibits the invasion and migration of GBM cells both *in vitro* and *in vivo* by suppressing the *WNT/β-catenin* signaling pathway (Scheme 1). Our results demonstrate that BPNS directly binds to CSNK2A2, reducing its kinase activity, which, in

* Corresponding authors.
E-mail addresses: liugan5@mail.sysu.edu.cn (G. Liu), dengwb5@mail.sysu.edu.cn (W. Deng).

https://doi.org/10.1016/j.cej.2024.148614
Received 5 September 2023; Received in revised form 4 December 2023; Accepted 5 January 2024
Available online 6 January 2024

turn, increases GSK-3β activity. Consequently, GSK-3β promotes β-catenin degradation, leading to the inhibition of the *WNT/β-catenin* signaling pathway and downregulation of key downstream genes like *Axin2*, *CD44*, and *Notch1*. The reduced *Notch1* levels inhibit the *NOTCH* pathway, further downregulating *Jag1*, *Hes1*, and *Akt1*. Overall, this study uncovers BPNS's inhibitory effect on invasion and migration in GBM cells and reveals the underlying molecular mechanism, offering potential avenues for future GBM treatments.

2. Materials and methods

2.1. Materials

The bulk BP crystals were purchased from Mukenano. N-methylpyrrolidone (NMP) was purchased from Aladdin. Fetal bovine serum was purchased from Cellcook. Penicillin-streptomycin, trypsin-EDTA, Dulbecco's Modified Eagle Medium (DMEM), Phosphate buffered saline (PBS), Triethanolamine buffered saline solution (TBS) were purchased from Gibco. The antibodies information of primary and secondary are fully listed in **Table. S1**. The relative primers of various genes in this article were purchased from TsingkeBiotechnology which were listed in **Table. S2**. Cell Counting Kit-8 was purchased from APExBIO. PMSF, 4% paraformaldehyde and DAPI were purchased from SolarBio (Beijing Solarbio Science & Technology Co., Ltd.). Coumarin 6 and RIPA lysis buffer were purchased from MCE. Western transfer fluid was purchased from Beyotime Biotechnology. Omni-Easy ^{TM} One-Step PAGE Gel Fast Preparation Kit (10%) and 5 × Protein Loading Buffer were purchased from Shanghai EpiZyme Biomedical Technology Co., Ltd. Lipofectamine 2000 was purchased from Invitrogen. TRIzol and 2 × Laemmli sample buffer was purchased from Sigma. D-luciferin was purchased from Glpbio Technology. Matrigel was purchased from BioCoat. SiCSNK2A2 was purchased from RIBOBIO. CHIR 99021 and XAV939 were purchased from STEM CELL. IR780 was purchased from ALORICH. LiCl was purchased from MACKLIN.

2.2. The preparation of BPNS

Black phosphorus nanosheets (BPNSs) were prepared through liquid exfoliation of bulk black phosphorus crystals. Initially, 30 mg of lump black phosphorus was ground in a mortar with the solvent NMP. The resulting suspension was transferred to a 100 mL blue-neck bottle and topped up with NMP to a total volume of 60 mL. The liquid phase exfoliation was carried out in an ice-water bath using an amplifier (Amplifier: 25 %, On/Off cycle: 5 s/5 s) for 12 h. Afterward, the peeling system was placed in an ultrasonic machine and subjected to constant low-temperature water bath for 8 h using an ultrasonic processor (EMERSON, Mexico). Following this process, the suspension was centrifuged at 7000 rpm and 4°C for 10 min to discard the precipitate (unpeeled black phosphorus) and retain the supernatant. The supernatant was then centrifuged at 10,000 rpm and 4°C for 10 min to collect the precipitate (BPNS), which was dispersed in NMP and stored at 4°C for future use.

2.3. Characterization of BPNS

The morphology of BPNS was characterized using Transmission Electron Microscope (TEM) (JEOL JEM-2010HR, Japan) and Atomic Force Microscope (AFM) (Bruker Dimension ICON, Massachusetts, USA). TEM was operated at an accelerating voltage of 200 kV, while AFM was performed using tapping mode in the air. Dynamic light scattering (DLS) was used to measure the size and electrical properties of BPNS. To prepare the sample, 10 μg of BPNSs were washed three times with double distilled (dd) water, dispersed in 2 mL of dd water, and then analyzed using a NanoBrook 90PlusPALS (Brookhaven Instruments, USA).

2.4. Growth inhibition assays

In order to determine an appropriate administration window, we conducted growth inhibition experiments on tumor cells and healthy brain cells. The growth inhibition effects of BPNS on U87-MG, GL261, neuron progenitor cells (NPC), and BV2 cells were evaluated using the Cell Counting Kit-8 assays (CCK-8). Briefly, the cells were seeded on 96-well plates (5 × 10^3 cells per well) with 100 μL of the DMEM culture medium supplemented with 10 % FBS and cultured overnight. The culture medium was replaced by 100 μL of the fresh medium containing different concentrations of BPNS (0, 1, 2, 4, 8, 16, 32 μg/mL) and cultured for 24 h. The corresponding concentrations of BPNS dispersed in the complete medium was used as the blank group. For the GL261 cells requiring NIR radiation, after being treated with BPNS for 1 h, NIR

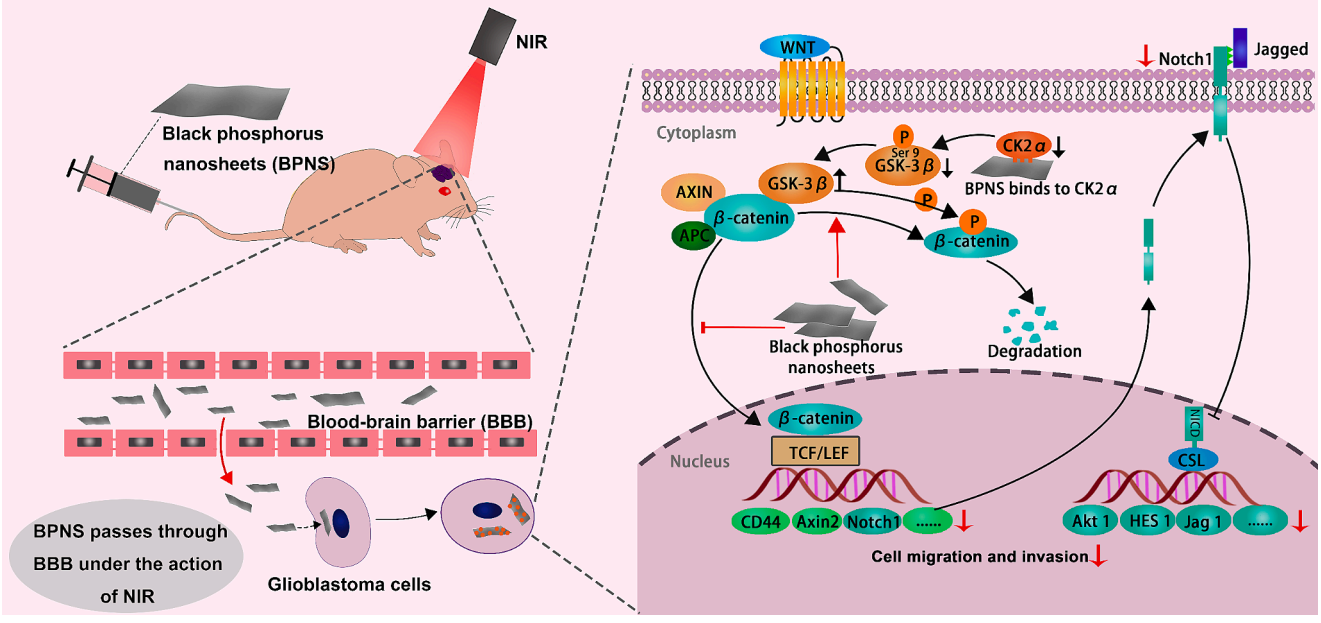

Scheme 1. The schematic diagram illustrates the underlying biological mechanisms through which BPNS inhibits the migration and invasion of glioblastoma.

irradiation (1 W/cm^2) was applied for 10 min, and then the samples were placed in the incubator for further cultivation. Afterward, 10 μL CCK-8 working solution was added to each well and incubated for 1 h in an incubator. The absorbance was measured at 450 nm to examine the relative number of viable cells, and the absorbance of the untreated cells cultured under the same conditions was used as a reference representing 100 % cellular viability by a multi-function plate reader (PerkinElmer, Finland). The percentage of cell viability was calculated using the following formula: Cell viability (%) = ($OD_{BPNS\ treated} - OD_{BPNS\ blank}$)/($OD_{control} - OD_{blank}$) × 100 %.

2.5. Cell migration and invasion assays

The unique feature of glioblastoma cells compared to other cells is their intrinsic invasiveness. To explore whether BPNS affects the characteristics of GBM, we conducted the following experiments. U87-MG and U251-MG cells were separately seeded in 12-well plates. When the cell density reached 90 %, a wounding line was created by scratching the cells with a 200 μL pipet tip. The cell debris was washed away with PBS and basic culture medium with different concentrations of BPNS (0, 1, 2, 4, 8 μg/mL) was added. After incubation for 48 h, cell migration results were monitored with an Olympus inverted microscope and analyzed with ImageJ. The cell migration ability of GL261 cells was also explored using the same method as the U87-MG cells, except BPNS was dispersed in complete medium instead of serum-free medium. The data were obtained from three independent experiments.

U87-MG and U251-MG cells were respectively seeded in an ultra-low adsorption 96-well plate at the density of 4000 cells per well. After incubating overnight, the formed 3D tumor sphere was transferred to 96-well plates that were coated with Matrigel, added BPNS, and photographed at different time points (0 h, 24 h, 48 h).

Trans-well filters (6.5 mm diameter, 8.0 μM pore size, Corning) were pre-coated with Matrigel for 1 h. Cells were harvested and seeded into the upper chamber at a density of 1×10^5 cells per well with serum-free medium. The lower chamber was added with 800 μL of fresh medium containing 30 % fetal bovine serum. After 48 h of incubation, the medium was collected, and the cells on the lower surface of the upper chamber were digested with 0.25 % trypsin. The digestion was stopped with the collected medium, and the cells were centrifuged at 1000 rpm for 5 min, resuspended in 100 μL of fresh medium, and counted with a cell counter. The number of living cells was then calculated, and the data were statistically analyzed with GraphPad Prism 5. For the experiments investigating the effects of XAV 939 and CHIR99021 on the invasion and migration in *WNT/β-catenin* signaling pathway of glioblastoma cells, the procedures were carried out similarly to the above-mentioned experiments.

2.6. In vivo BBB transportation and biosafety of BPNS

In order to verify whether BPNS can penetrate the blood–brain barrier (BBB) with the assistance of NIR, we conducted experiments using nude mice with intact BBB integrity. We used two methods to validate whether BPNS crossed the BBB. First, we reacted IR780 and BPNS in a 5:1 mass ratio in NMP, incubated at room temperature for 48 h, washed 3 times with NMP, and then washed with sterile water to remove unbound IR780. BPNS-IR780 was dispersed in saline for later use. Healthy mice were divided into three groups: Ctrl group, BPNS-IR780 group, and BPNS-IR780 + NIR group. They were respectively injected with 100 μL saline, 100 μL BPNS-IR780, and 100 μL BPNS-IR780 via the tail vein. Subsequently, the mice were anesthetized with 1 % pentobarbital sodium, exposed to NIR (1 W/cm^2) in the BPNS-IR780 + NIR group, and the temperature was monitored using a thermal imaging camera. After 3 h, the brains of the mice in each group were taken, and the experimental results were detected using *in vivo* imaging (PE IVIS Luminna III, USA).

Second, healthy mice were divided into two groups: the Ctrl group and the BPNS + NIR group. The Ctrl group of mice received a tail vein injection of 100 μL of saline and was subjected to NIR (1 W/cm^2) irradiation for 5 min. The experimental group of mice received a tail vein injection of BPNS and was subjected to the same NIR (1 W/cm^2) irradiation for 5 min. During the NIR irradiation, a near-infrared thermal imaging device was used to detect the temperature changes and keep the temperature around 42°C. After 30 min, the mice's brains were removed, and NIR irradiation (1 W/cm^2) was used to assess the temperature increase in different brain regions, indicating whether BPNS had crossed the BBB.

To evaluate whether the thermal effect produced by BPNS under NIR would cause damage to the brain, healthy nude mice were divided into four groups: Ctrl group, NIR group, BPNS group, and BPNS + NIR group. The Ctrl group received a tail vein injection of 100 μL of saline. The NIR group received a tail vein injection of saline followed by 5 min of NIR irradiation (1 W/cm^2). The BPNS group received a tail vein injection of BPNS dispersed in 100 μL saline at a dose of 0.56 mg/kg. The BPNS + NIR group received a tail vein injection of BPNS followed by 5 min of NIR irradiation (1 W/cm^2). The administration was performed once every other day, and after five administrations, the brains of the mice were collected for H&E staining.

2.7. Subcutaneous and orthotopic xenografts implantation

All animal experiments were performed in accordance with the specifications of the Laboratory Animal Center, Sun Yat-sen University, and were approved by the Institutional Animal Care and Use Committee (IACUC), Sun Yat-sen University. The approved number was No. SYSU-IACUC-2021–000581. Balb/c nude mice (4–6 weeks, 18–20 g, male) were used for the subcutaneous tumor model. U87-MG cells were cultured and harvested, and the cells were resuspended in PBS to a concentration of 1×10^7 cells/mL. Subsequently, 100 μL of the U87-MG cell suspension was subcutaneously inoculated on the right inguinal region of each mouse. When the tumor volume of the mice reached 100 mm^3, BPNS was dispersed in physiological saline and administered to each mouse via intravenous injection at a dose of 0.56 mg/kg. The experimental group received BPNS administration every other day, for a total of 7 doses before stopping the treatment. The control group received an equivalent volume of physiological saline via intravenous injection at the same time intervals. After removing the subcutaneous tumor, a part of the frozen tissue was used to extract protein and mRNA, while the other part was used for immunohistochemistry. The main organs were removed and stored in 4 % paraformaldehyde for H&E staining and Masson staining to evaluate the biological safety of BPNS. The formula of tumor volume growth rate = ($V-V_0$)/V_0.

Balb/c nude mice (4–6 weeks, 18–20 g, male) were used for the orthotropic glioma model. Male nude mice were anesthetized with 1 % sodium pentobarbital, and 5×10^5 of GL261-Luc cells were implanted into the right brain, 1.8 mm lateral and 0.6 mm anterior to the bregma, at a depth of 2.5 mm, using a brain stereotaxic device. On day 10, the mice were randomly divided into four groups: Control group, NIR group, BPNS group, and BPNS + NIR group. D-luciferin was intraperitoneally injected at a dose of 3 mg/20 g for *in vivo* imaging to observe the tumor progression every 4 days. The BPNS + NIR group received an intravenous injection of BPNS with a dosage of 0.56 mg/kg every 2 days, was anesthetized with 1 % sodium pentobarbital, and illuminated for 5 min under NIR (1 W/cm^2). The BPNS group received an intravenous injection of BPNS with a dosage of 0.56 mg/kg every 2 days, and was anesthetized with 1 % sodium pentobarbital. The NIR group received an intravenous injection of physiological saline every 2 days, was anesthetized with 1 % sodium pentobarbital, and was illuminated for 5 min under NIR (1 W/cm^2). The Control group (Ctrl group) received an intravenous injection of physiological saline every 2 days and was anesthetized with 1 % sodium pentobarbital. After another 10 days, two mice from each group were randomly selected, overdosed with anesthesia, and had their brains removed for H&E staining. The survival time

of the remaining mice was observed and recorded. The formula of body weight change rate = $(M-M_0)/M_0$.

2.8. RNA-sequencing assay

U87-MG cells were seeded on 6-well plates at a density of 1×10^6 cells and incubated overnight. After the density reached 60 %-70 %, BPNS was dispersed in fresh medium and added to the experimental group. The cells were digested with 0.25 % trypsin, washed with pre-cooled PBS, collected the cells and added with 0.5 mL of TRIzol to each sample. The samples were then subjected to Illumina high-throughput sequencing. RNA-sequencing data were obtained from four independent samples.

2.9. Quantitative real-time PCR (qRT-PCR)

qRT-PCR was used to detect the mRNA expression of U87-MG, tumor tissue under the influence of BPNS. Cells were seeded in 6-well plates and incubated when the density reached about 70 %, added 4 μg/mL of BPNS, and incubated for 24 h, while the untreated well was used as a control group. Total RNA extracted from the cultured cells by RNA Quick Purification Kit (EZBioscience). cDNA was reverse transcribed from 1.0 μg RNA with EasyScript® All-in-One First-Strand cDNA Synthesis SuperMix for qPCR (One-Step gDNA Removal) (TransGen). The mRNA levels of relative gene were detected by quantitative real-time PCR which performed with PerfectStart Green qPCR SuperMix (TransGen). The result was detected at LightCycler 96 Real-Time PCR Detection System (Roche LightCycler96, Switzerland). Fold changes in relative gene expression were calculated by comparative Ct method (fold change = $2^{-\Delta\Delta Ct}$). qRT-PCR analysis of the relative mRNA expression was detected and statistically analyzed by LightCycler software.

2.10. Western blotting assay

Western blotting (WB) was used to detect the protein expression of U87-MG, GL261 cells, U251-MG, and tumor tissue after the treatment of BPNS. The cells were seeded in 6-well plates and incubated until the density reached about 70 %. Then, 4 μg/mL of BPNS was added, and the cells were incubated for 24 h. The untreated wells were used as the control group. To obtain whole-cell protein, the cells were digested with 0.25 % trypsin, washed with phosphate-buffered saline (PBS), and lysed with PMSF-containing RIPA buffer to prevent protein degradation. The cells were cleaved on ice for 30 min, centrifuged at 12000 rpm for 10 min, and the supernatant was collected. After quantifying the whole proteins with a Bradford kit, the proteins were denatured in loading buffer by boiling at 100°C for 10 min. Next, equal amounts of proteins were separated by 10 % SDS polyacrylamide gel electrophoresis and transferred onto a polyvinylidene difluoride (PVDF) membrane (0.2 μm). The membrane was blocked in 5 % milk for 2 h, washed 3 times with 1 × TBST for 10 min each, and then incubated with the primary antibody. Specific antibodies against p-GSK-3β, β-catenin, GSK-3β, p-β-catenin, cyclin D1, c-Myc, cyclin D3, Sox 2, CD44, cyclin D1, Notch1, Jag1, CSNK2A2, Hes1, and GAPDH (1:1000) were used to detect the corresponding protein expression. After the PVDF membrane was washed by 1 × TBST for 3 times, the corresponding secondary antibodies were added to incubate for 2 h, and then washed 3 times with 1 × TBST for 10 min each time. Immunoblots were detected through Western-Bright™ Peroxide (Advansta) and exposed by BG-gds AUTO Image System (BG-GDAAUTO0730, Beijing, China). The ImageJ was used to analyze the relative expression level of protein.

2.11. Immunofluorescence experiment

Immunofluorescence was used to detect the expression of β-catenin, CD44, Notch1, and CSNK2A2. U87-MG cells were seeded in a 12-well plate with glass slides inside at the density of 5×10^4 cells/mL. After the cells adhered to the slide, treated with 4 μg/mL BPNS for 24 h. Then the cells on coverslips were fixed with 4 % paraformaldehyde, blocked with 5 % milk, incubated with primary antibodies (β-catenin 1:200; CD44 1:200; Notch1 1:200; CSNK2A2 1:200) and corresponding fluorescence-labeled secondary antibodies. The nucleus was stained with DAPI and examined with Zeiss LSM 780 Meta confocal microscope (Germany). The images were processed by ZEN software.

2.12. BPNS binding intracellular proteins assay

For LC-MS/MS identification, 100 μg of BPNS was incubated with U87-MG cell lysates (5 mg) in the binding buffer containing 50 mM Tris-HCl pH 7.4, 150 mM NaCl and 1 mM EDTA in a total volume of 1 mL at 4°C overnight. Then, BPNS was washed 5 times with the binding buffer, collected by centrifugation, and the obtained solution was concentrated. The proteins that were bound with BPNS were enzymatically cleaved. Subsequently, LC-MS/MS (Thermo QE-HF/QE- HF-X, Germany) analysis was performed to obtain highly reliable protein peptide sequences. These sequences were then compared against a protein database to obtain protein identification (ID).

For pull down assay, 10 μg of BPNS was incubated with U87-MG cell lysates (500 μg) in the binding buffer in a total volume of 1 mL at 4°C overnight. Then, BPNS was washed 5 times with the binding buffer, collected by centrifugation, and boiled with 1 × Laemmli sample buffer. The samples were analyzed by immunoblotting.

For the BPNS binding intracellular proteins assay, we cultured U87-MG cells in a 10 cm dish. After the cell density reached approximately 70 %, the medium was replaced with fresh medium containing 4 μg/mL of BPNS, and the cells were cultured continuously for 24 h. The cells were collected and lysed using RIPA buffer containing a phosphatase inhibitor, followed by centrifugation at 12,000 rpm for 10 min to collect the precipitate. Subsequently, the obtained BPNS precipitate was washed with 1 × binding buffer, and then processed as a protein sample and used for Western blot experiments.

2.13. Colocalization experiment

BPNS and coumarin 6 (C6) were dispersed in NMP at a mass ratio of 1:3. The dispersion was stirred at room temperature for at least 24 h. The complex (BPNS-C6) was centrifuged at 12,000 rpm for 10 min and washed twice with NMP, followed by one wash with anhydrous ethanol and one wash with sterile water. Subsequently, BPNS-C6 was dispersed in complete culture medium. Pre-coated slides were seeded with U87-MG cells in a 12-well plate, and the BPNS-C6 was added to the experimental group. The wells without any treatment, only replaced with fresh complete culture medium, were used as the control group. The 12-well plate was then placed in a cell culture incubator and further incubated for 12 h. This was followed by the immunofluorescence staining step. After staining with the secondary antibody and mounting the slides, the results could be detected by confocal microscopy.

2.14. Gene knockout experiment

U87-MG cells were seeded in a 6-well plate and cultured in antibiotic-free complete medium. Once the cells reached 40–50 % confluency, they were ready for transfection experiments. 5 nmol of st-h-CSNK2A2 was dissolved in RNase-free water to prepare a 20 μM stock solution. A solution was prepared by dispersing 5 μL of lipofectamine 2000 transfection reagent in 200 μL of DMEM, thoroughly mixing, and letting it stand at room temperature for 5 min. B solution was prepared by combining 5 μL of siCSNK2A2 stock solution with 200 μL of DMEM, mixing well. A and B solutions were mixed together thoroughly and allowed to stand at room temperature for 20 min to obtain the transfection mixture. The culture medium in the 6-well plate was removed, and the cells were washed once with PBS. Then, 1.6 mL of DMEM was

added followed by adding 400 μL the transfection mixture. The plate was gently shaken to ensure proper mixing. Corresponding control group were set up as needed for the experiment. The 6-well plate was placed in a CO_2 incubator at 37°C. After 5–6 h incubation, the culture medium was replaced with complete medium, and the cells were cultured for an additional 48 h. Subsequently, cellular proteins were extracted for next experiments.

2.15. Statistical analysis

All data were expressed as the mean ± SD. Statistical analysis was done using paired *t-test* with GraphPad Prism 5 software, except described otherwise. Differences were considered significant when *P* values were < 0.05. The *P* values of < 0.05, < 0.01 and < 0.001 were indicated as *, **, and ***, respectively.

3. Results

3.1. BPNS could effectively inhibit the invasion and migration of glioblastoma cells in vitro

In our study, we employed liquid-phase exfoliation to prepare BPNS from bulk black phosphorus, followed by gradient centrifugation to obtain BPNS centrifuged at 7000 rpm-10000 rpm. The morphology of BPNS was characterized by Transmission Electron Microscope (TEM), Atomic Force Electron Microscope (AFM) and DLS (Dynamic Light Scattering). As shown in Fig. S1**A-B**, BPNS presented a sheet structure with an average lateral size of 200 nm and an average thickness of 12 nm from TEM and AFM results. These results were consistent with the DLS measurement in Fig. S1**C-D**, reporting that the particle size of BPNS was around 200 nm and the surface charge was around −27 mV. Further, BPNS was dispersed in different dispersant systems and observed at different time points. The dispersion experiment results showed that in PBS, BPNS exhibited significant sedimentation, while in H_2O and complete culture medium, BPNS showed good dispersion, as shown in Fig. S1**E**.

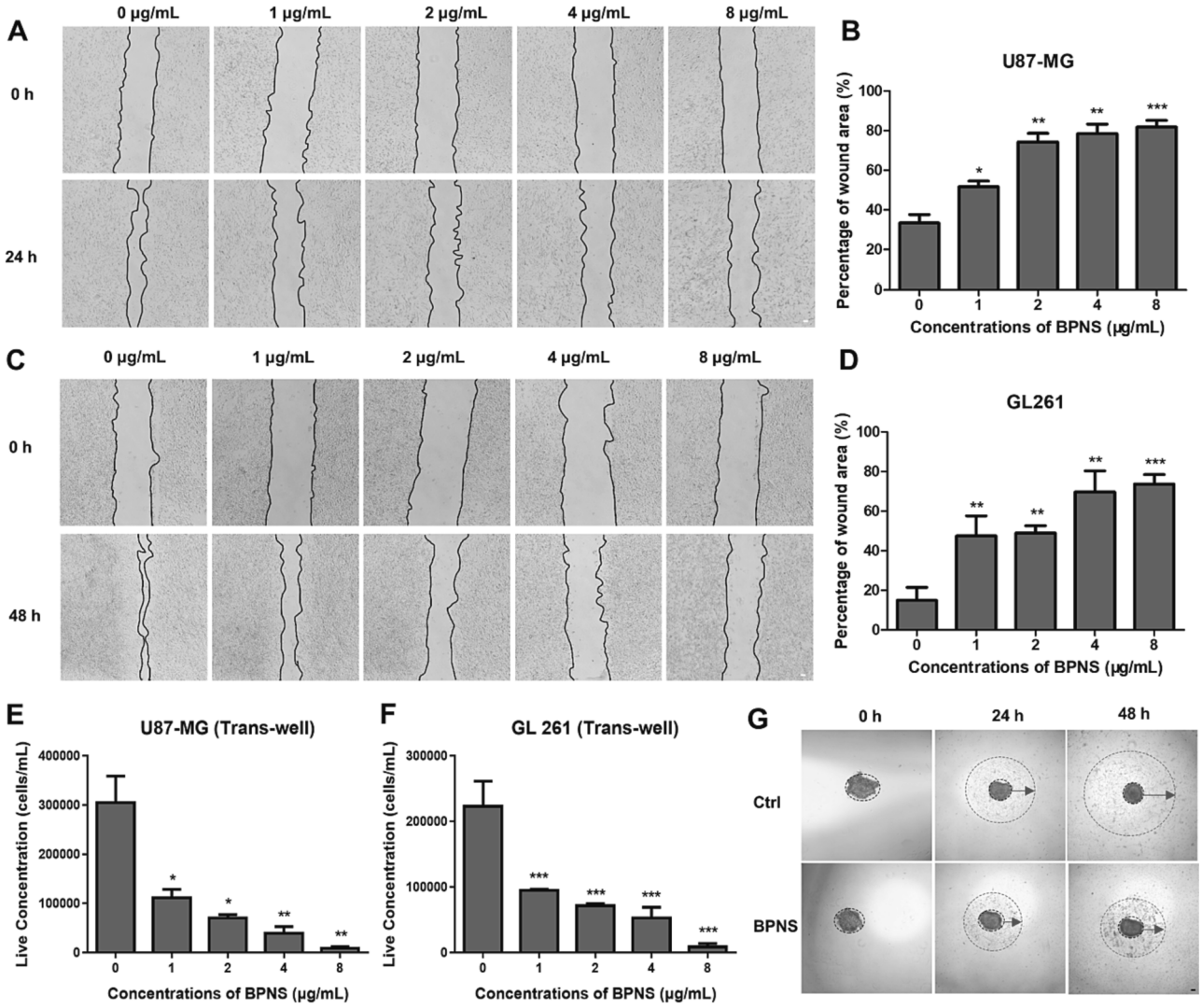

Fig. 1. BPNS inhibited the invasion and migration of glioblastoma cells. (A) A wound-healing assay results of U87-MG cells which treated with BPNS (0, 1, 2, 4, 8 μg/mL) for 24 h. (B) The quantitative statistical results of the U87-MG cell wound-healing assay ($n = 3$). (C) GL261 cells were treated with BPNS for 48 h to evaluate cell migration ability by wound-healing assay. (D) The quantitative statistical results of the GL261 cell wound-healing assay. ($n = 3$). (E) The *trans*-well results of U87-MG cells after being treated with different concentrations of BPNS ($n = 3$). (F) The *trans*-well results of GL261 cells after being treated with different concentrations of BPNS ($n = 3$). (G) 3D cell spheroid invasion assay results of U87-MG cells after being treated with BPNS for 24 h and 48 h. Scale bar: 100 μm. Error bar, mean ± SD, $^*P < 0.05$, $^{**}P < 0.01$, $^{***}P < 0.001$.

To investigate the impact of BPNS on the viability of normal brain cells and glioblastoma cells and determine the range of administration. Glioblastoma cells (U87-MG, GL261) and normal brain cells (BV2, NPC) were used as experimental subjects. The CCK-8 results showed that BPNS inhibited the proliferation of tumor cells in a concentration-dependent manner and exhibited significant toxic effect on normal brain cells at concentrations greater than 8 μg/mL, so we adopted lower concentrations (1 to 8 μg/mL) for subsequent experiments (Fig. S1**F**).

Migration and invasion of glioblastoma cells are well-known dominating factors, causing treatment failure of glioblastoma patients. Then, we detected whether BPNS could inhibit the migration and invasion of glioblastoma cells by the wound-healing assay, *trans*-well assay, and three-dimensional (3D) tumor spheroid assay[28]. As shown in Fig. 1A-D and Fig. S2**A-B**, the percentage of wound area in U87-MG, GL261 and U251-MG cells was significantly raised after being treated with BPNS in a concentration-dependent manner. We obtained BPNS of different sizes (around 650 nm, around 260 nm, around 180 nm) through gradient centrifugation (1000 rpm-4000 rpm, 4000 rpm-7000 rpm, 10000 rpm-14000 rpm) to preliminarily verify whether the size of BPNS affects its migration ability. The results of scratch experiments on U87-MG cells indicated that BPNS of different sizes exhibited a similar inhibitory effect on the migration ability of glioblastoma cells (Fig. S3). Then, *trans*-

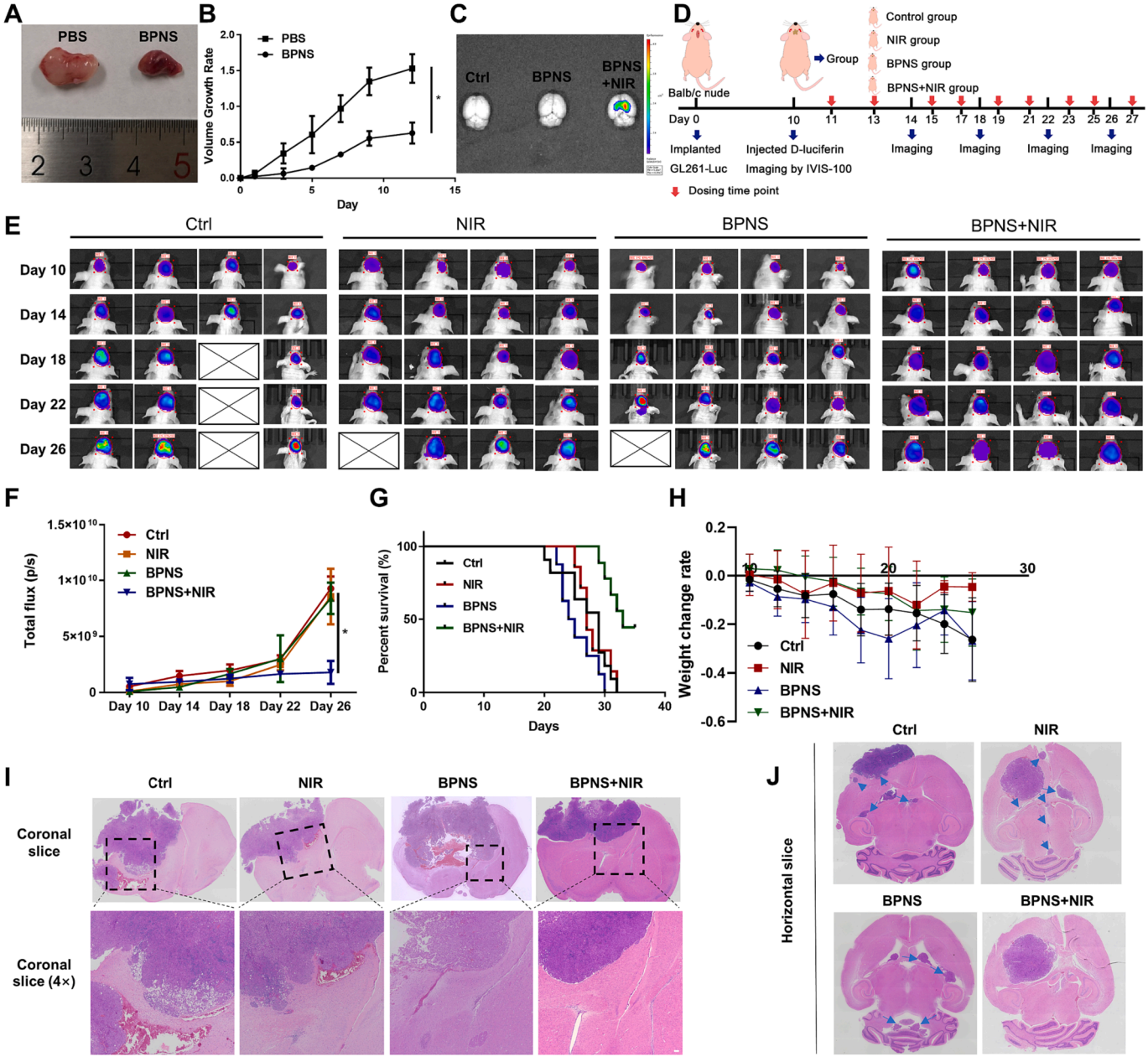

Fig. 2. *In vivo* experiments were conducted to verify the bioactivity of BPNS. (A) Representative image of tumor tissue size after treated with PBS and BPNS. (B) The tumor growth curve of tumor-bearing mice treated by PBS or BPNS ($n = 3$). (C) The fluorescent imaging of the brains after BPNS labeled with IR780 to verify whether BPNS could cross BBB in different group: Ctrl group, BPNS-IR780 group, BPNS-IR780 + NIR group. (D) The illustration of the orthotopic glioblastoma experimental process. (E) *In vivo* imaging results showed the changes in tumor progression in different groups over time. (F) Statistical results were obtained for the bioluminescence intensity at different time points in each group. (G) Survival curves were created for each group of mice ($n = 7$). (H) The body weight change rate of mice in each group during the whole treatment. (I) H&E staining of the coronal section in the part of the striatum. (J) H&E staining of the horizontal section, and the blue arrows indicate the location of tumor metastasis. Error bar, mean ± SD, $^*P < 0.05$. Scale bar: 100 μm. (For interpretation of the references to colour in this figure legend, the reader is referred to the web version of this article.)

well assay and three-dimensional (3D) tumor spheroid invasion assay was conducted to evaluate the cell invasion ability of glioblastoma cells after being treated with BPNS. As shown in Fig. 1E-F and Fig. S4**A-B**, tumor cells transferred to the bottom wells were significantly decreased in the presence of BPNS. Consistently, the observation of the distance of cell invasion outward on 3D tumor spheroids also indicated that BPNS inhibited the invasion of glioblastoma cells (Fig. 1G and **Fig. S5**). Results above collectively revealed that BPNS could effectively inhibit the invasion and migration of glioblastoma cells *in vitro*.

3.2. BPNS inhibited the growth, invasion, and migration of GBM in vivo

To determine whether BPNS has an intuitively inhibitory effect on glioblastoma *in vivo*, a xenograft tumor model was established by subcutaneously injecting U87-MG cells into the right flank of nude mice. The growth of subcutaneously transplanted tumors derived from U87-MG cells was significantly suppressed after treatment with BPNS compared to the blank control group. As shown in Fig. 2A-B, the tumor volume in the BPNS group was significantly smaller than that in the PBS group. Meanwhile, the body weight change rate of the mice (Fig. S6**A**), the H&E staining results (Fig. S6**B**), and the MASSON staining results (Fig. S6**C**) in both the control and BPNS groups did not show a significant difference, indicating that the dosage of BPNS has a therapeutic effect on glioblastoma without sever toxic side effects.

There are studies indicating that under the assistance of NIR, the permeability of BBB can be improved by BPNS[21–23]. According to the methods described in the literature, we adopted the following method to verify this point. As shown in **Fig. S7A**, the brain temperature of the experimental group mice was higher compared to the control group, and it remained around 42°C. The temperature difference of nearly 3°C was also be observed from the extracted brain samples from the BPNS group and the control group which inferred that BPNS crossed the BBB under the influence of NIR and accumulated in the brain tissue. NIR fluorescence imaging was also performed with IR780 labeled BPNS (BPNS-IR780). For the mice treated with BPNS-IR780 under NIR laser irradiation, the brain fluorescence intensity was significantly higher than that of other groups (Fig. 2C **and Fig. S7B**). These results showed that under NIR irradiation, BPNS exhibited photothermal effects and was capable of crossing the BBB. Furthermore, the results of brain H&E staining experiments conducted on healthy mice in different treatment groups also indicated that NIR irradiation did not cause damage to the brain (**Fig. S7C**).

Then we established an orthotopic glioblastoma model to verify whether BPNS could inhibit the migration and invasion of glioblastoma *in vivo*[29]. According to our previous proliferation activity assay, BPNS at a concentration of 4 μg/mL exhibited a slight inhibitory effect on GL261 cells. As shown in the Fig. S1**F**, the average proliferation activity of GL261 cells was approximately 95 %. Furthermore, CCK-8 experiments confirmed that the combination of BPNS and NIR irradiation had no significant impact on the viability of GL261 cells. As shown in the **Fig. S7D**, the average cell viability of GL261 cells, after treatment with BPNS and combined NIR irradiation, remained above 92 %. These collective observations suggested that the tumor proliferation inhibitory effect induced by BPNS can be disregarded in the tumor model based on GL261 cells, which indicated that GL261 cells were a suitable choice for establishing an orthotopic glioblastoma model, and suggested that the administered concentration primarily manifested its biological activity in inhibiting the invasion and migration of glioblastoma cells. The animal experiment workflow was summarized in Fig. 2D. *In vivo* imaging results demonstrated a substantial decrease in the total fluorescence intensity of the BPNS + NIR group compared to other three groups on Day 26, providing clear evidence of the tumor inhibition effect exerted by BPNS (Fig. 2E-F). The survival time statistics also showed that the treatment of BPNS + NIR could prolong the survival time of tumor-bearing mice without effect on body weight (Fig. 2**G-H**). Further, H&E staining of brain slices were performed to morphologically observe the metastasis of GBM. The coronal slice staining images showed that tumor cells were invading normal tissue in the control group (Fig. 2I), while tumor margins in the BPNS + NIR group were smoother which indicated a decrease in trace of the invasion. In the horizontal slices of H&E staining (Fig. 2J), it could be also observed that tumors had migrated from the lesion and spread to various parts of the brain in the untreated group, while the BPNS + NIR treated tumors remained in the lesion, indicating that the invasion and migration of glioblastoma cells were effectively inhibited by BPNS. These all suggested BPNS showed an inhibitory effect on the invasion and migration of glioblastoma cells *in vivo*.

Finally, to further evaluate the dosage administration safety of BPNS *in vivo*, we stained the major organ tissues from orthotopic glioma mice with H&E and MASSON. The staining results showed no significant tissue damage in either the control or BPNS-treated groups (**Fig. S8-S9**). Collectively, our results showed BPNS inhibited the growth, migration, and invasion of GBM without a high system toxicity.

3.3. RNA sequencing revealed WNT/β-catenin signaling pathway may participate in the BPNS mediated inhibition of migration and invasion of glioblastoma cells

Next, we performed RNA sequencing to uncover the underlying molecular mechanisms. The pathway enrichment analysis of RNA sequencing revealed that the differentially expressed genes (DEG) were mainly enriched in extracellular matrix (ECM)-related pathways (Fig. 3A). These ECM-related pathways collectively participate in the complex process of regulating cell behavior, such as proliferation, migration, and other processes, which further suggest that BPNS has biological activity that can affect the invasion and migration of glioblastoma. Moreover, heatmap of extracellular matrix-related DEG showed that BPNS mainly down-regulated the extracellular matrix-related genes, and qRT-PCR further confirmed this result (Fig. 3B-C). Additionally, Gene Set Enrichment Analysis (GSEA) software was also adopted to interpret the RNA sequencing data. Among the top 20 enriched gene sets (Nom p-val < 0.05, FDR p-val < 0.25) in HALLMARK, *WNT/β-catenin* signaling, which is closely related to most tumor cell invasion and migration[30,31], were included (Fig. 3D). The enrichment plot and DEG volcano-map both showed BPNS significantly downregulated *WNT/β-catenin* signaling-related genes, of which 160 genes were down-regulated and 55 genes were up-regulated under the influence of BPNS (Fig. 3E-F). A cross-analysis between the differential genes of the *WNT/β-catenin* signaling pathway and the genes related to invasion and migration showed that 47 genes were down-regulated, and 10 genes were up-regulated (Fig. 3G). These RNA sequencing analysis data suggested that BPNS inhibited the invasion and migration of glioblastoma cells probably through inactivating the *WNT/β-catenin* signaling pathway.

3.4. BPNS suppressed the migration and invasion of glioblastoma cells by blocking the WNT/β-catenin signaling pathways

Firstly, we verified whether *WNT/β-catenin* signaling pathway participated in invasion and migration of glioblastoma cells. We employed XAV 939, a *WNT/β-catenin* signaling inhibitor, to inactivate the *WNT/β-catenin* signaling pathway. As depicted in Fig. 4A-B, the wound-healing of U87-MG cell was significantly inhibited by XAV 939. Furthermore, the *trans*-well assay demonstrated a notable suppression of invasion by XAV 939 (Fig. 4C). Conversely, we employed CHIR 99021 to activate the *WNT/β-catenin* signaling pathway and found the migration and invasion of U87- MG cells were significantly promoted (Fig. 4D-F). These all indicated that the activation of *WNT/β-catenin* signaling pathway contributed to the migration and invasion of GBM and BPNS might exert its action through inactivating *WNT/β-catenin* signaling pathway.

Subsequently, we detected genes expression involved in *WNT/*

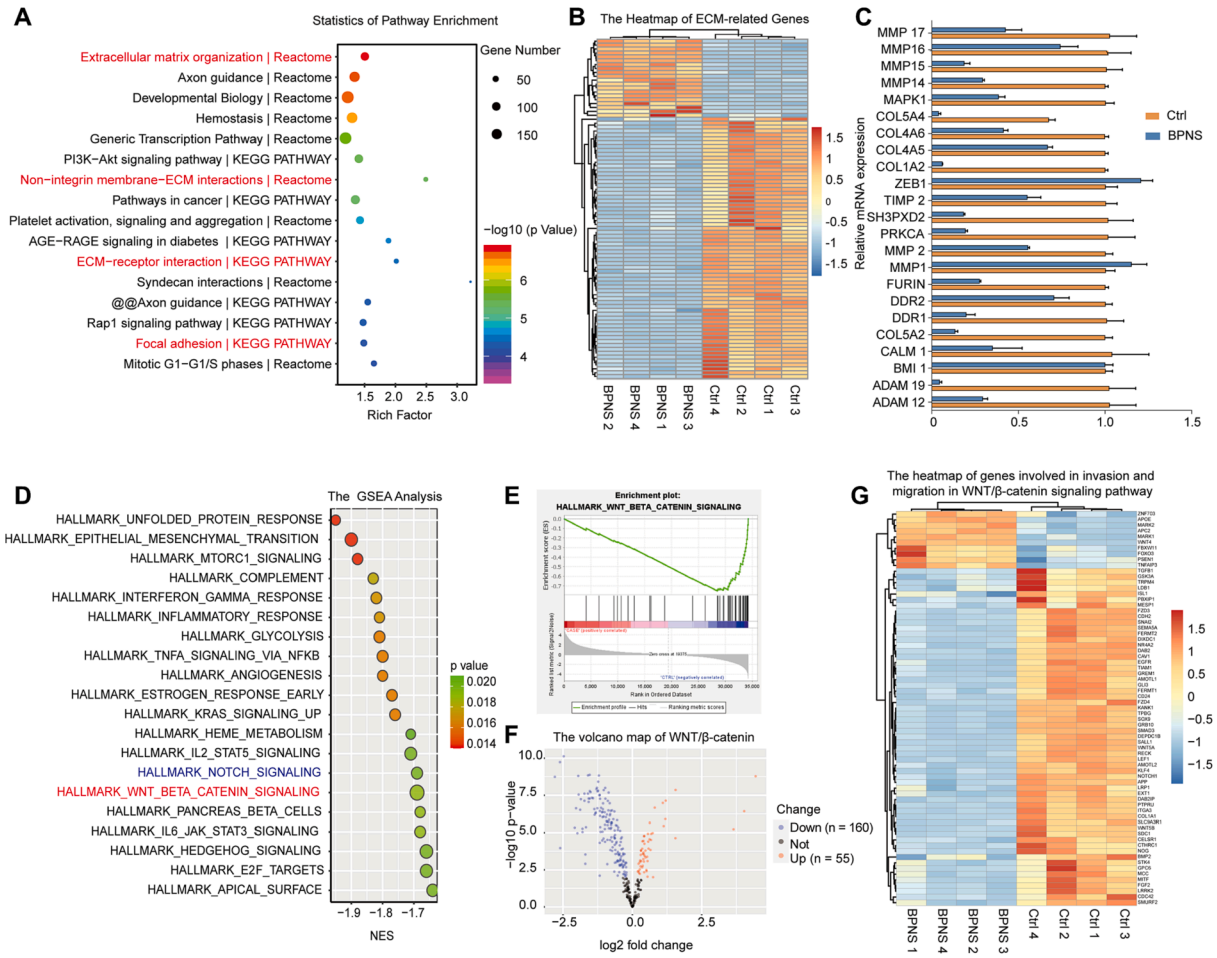

Fig. 3. The RNA sequencing analysis results and corresponding pathway enrichment analysis. (A) The statistic of pathway enrichment analysis results of U87-MG cells after treatment with BPNS for 24 h. (B) The heat map of extracellular matrix-related differentially expressed genes. (C) Genes expression of extracellular matrix-related detected by qRT-PCR. (D) The top 20 enrichment sets of GSEA analysis of U87-MG treated by BPNS versus untreated group. (E) Enrichment gene analysis of the *WNT/β-catenin* signaling pathway. (F) The volcano map of the genes in the *WNT/β-catenin* signaling pathway. (G) A cross-analysis between the differential genes of *WNT/β-catenin* signaling pathway and invasion and migration-related genes.

β-catenin signaling pathway after treated by BPNS. As shown in Fig. 4G, the downstream target genes of *WNT/β-catenin* signaling pathway were all significantly down-regulated after BPNS treatment, such as *c-Myc*, *Sox2*, *cyc D1*, *Notch1*, etc., and their corresponding proteins were down-regulated accordingly (Fig. 4H **and Fig. S10A-B**). β-catenin is a hub-biomarker used to judge whether the *WNT/β-catenin* signaling pathway is state-on. After BPNS treatment, the expression level of β-catenin in U87-MG was negatively correlated with the concentration of BPNS (Fig. 4**I-J**). For transcriptional activation of downstream genes of *WNT/β-catenin* pathway, β-catenin needs to enter the nucleus. Therefore, cellular localization of β-catenin was performed after cells were treated with BPNS. After treated with BPNS for 24 h, the fluorescence intensity of β-catenin in the nucleus area was indeed decreased compared to the control group (Fig. 4K-**L**). In normal circumstances, stabilized β-catenin can enter the cell nucleus and bind with TCF/LEF, enhancing its transcriptional activity. When the entry of β-catenin into the cell nucleus decreases, TCF/LEF may not fully exert its transcriptional activation function, resulting in a decrease in the expression level of target genes. TCF4 is an important member of the TCF/LEF transcription family and a crucial transcription factor in the *WNT/β-catenin* signaling pathway[32,33]. We detected the protein expression level of TCF4 using the immunoblotting method and found a significant down-regulation of TCF4 protein expression after BPNS treatment (**Fig. S10C-D**). The downregulation of downstream gene expression levels also indicated that BPNS inhibited the activity of this signaling pathway (Fig. 4G-**H**). We further studied the downstream targeting protein of the *WNT/β-catenin* signaling pathway to comprehensively understand the function of BPNS in glioblastoma cells. CD44, one of the downstream proteins of the *WNT/β-catenin* signaling pathway, is an important monitoring indicator that affects the invasion and migration ability of glioblastoma cells[34–37]. As shown in Fig. 4M-**N**, the expression of CD44 was significantly down-regulated in U87-MG after treated with BPNS for 24 h. Immunofluorescence results also showed the fluorescence intensity of CD44 in BPNS group was weaker than that of control group (Fig. 4O-**P**). BPNS has the same inhibitory effect on the *WNT/β-catenin* signaling pathway in two other glioblastoma cell lines (**Fig. S11**). These results revealed that BPNS inhibited the *WNT/β-catenin* signaling pathway by decreasing the protein level of β-catenin and preventing β-catenin from entering the nucleus to suppress the transcription of downstream genes.

3.5. *The inactivation of WNT/β-catenin signaling pathway induced by BPNS blocked the Notch1-mediated NOTCH signaling pathway*

In addition to the *WNT/β-catenin* signaling pathway, we also observed the *NOTCH* signaling pathway was also enriched in the top 20 enriched gene sets (Fig. 3D, blue font). The *NOTCH* signaling pathway was reported to regulate the transcription of cell migration and invasion, as well as the maintenance of glioblastoma stem cells[38–40]. The enrichment plot and DEG volcano-map both showed BPNS significantly

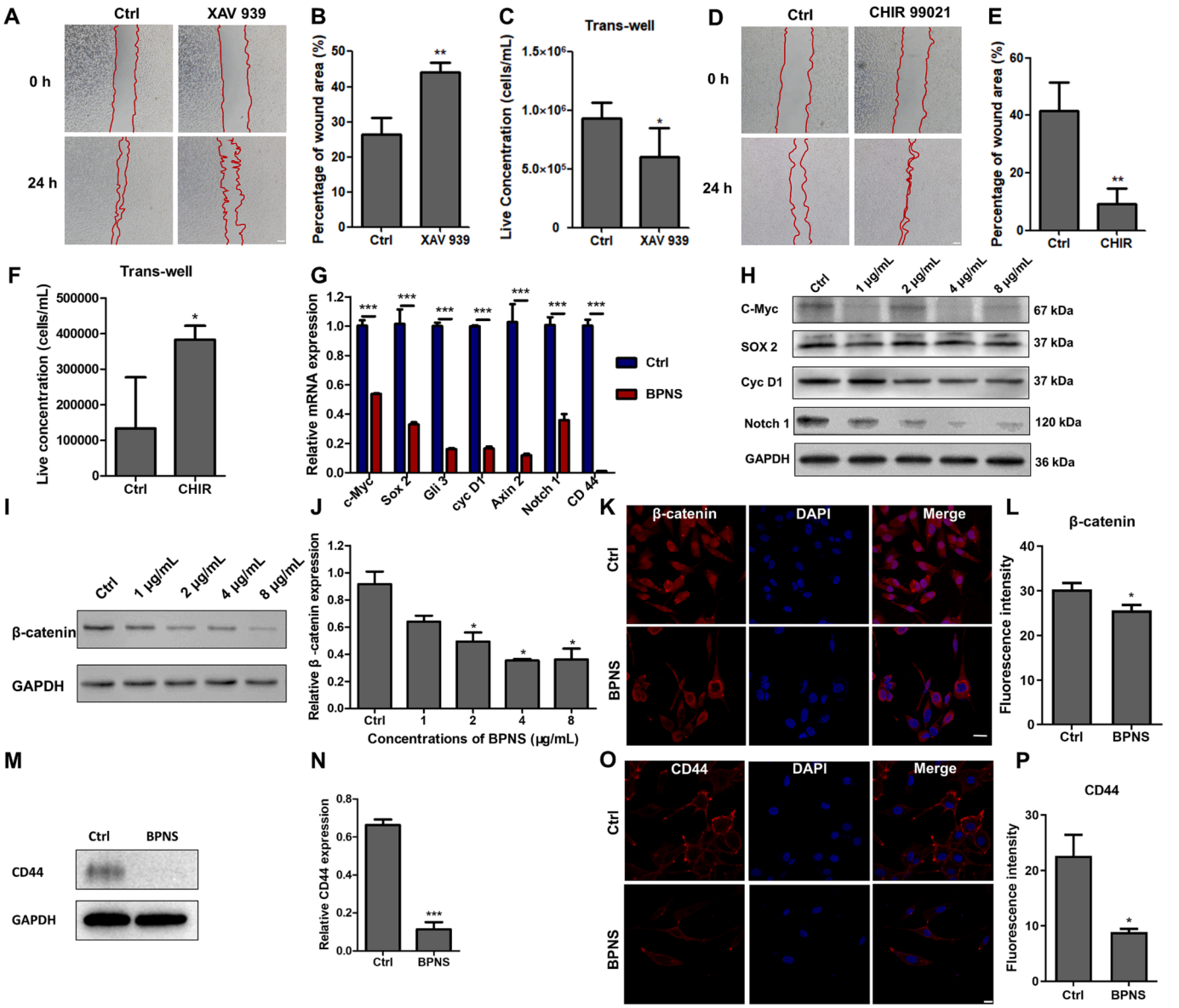

Fig. 4. BPNS inhibited the migration and invasion of glioblastoma cells by blocking the *WNT/β-catenin* signaling pathway. (A) A wound-healing assay results of U87-MG cells after treated with 1 μM XAV 939 for 24 h, scale bar: 100 μm. (B) The quantitative statistical results of wound-healing assay after the U87-MG cells treated with XAV 939 ($n = 3$). (C) The *trans*-well quantitative statistical results of U87-MG after treated with XAV 939. (D) A wound-healing assay results of U87-MG cells after treated with 10 nM CHIR 99021 for 24 h, scale bar: 100 μm. (E) The quantitative statistical results of wound-healing assay after the U87-MG cells treated with 10 nM CHIR 99021 ($n = 3$). (F) The *trans*-well quantitative statistical results of U87-MG after treated with 10 nM CHIR 99021. (G) The qRT-PCR results of *c-Myc*, *Sox2*, *CD44*, *Smad 3*, *cyc D1*, *Axin2*, *Notch1* of U87-MG cells after being treated with BPNS for 24 h. (H) The western blot results of c-Myc, Sox2, cyc D1, Notch1 of U87-MG cells after being treated with different concentrations of BPNS for 24 h. (I-J) The Western blot results and its quantification results of β-catenin after the cells were treated with BPNS in different concentrations for 24 h ($n = 3$). (K-L) The image of immunofluorescence and its corresponding quantitative statistics of β-catenin after U87-MG cells being treated with BPNS for 24 h, scale bar: 20 μm. (M−N) The Western blot results and its quantification results of the CD44 after the U87-MG cells treated with BPNS for 24 h. (O-P) The immunofluorescence image and its quantified data of CD44 after the U87-MG cells treated with BPNS for 24 h, scale bar: 20 μm. Error bar, mean ± SD, $^{*}P < 0.05$, $^{**}P < 0.01$, $^{***}P < 0.001$.

downregulated the *NOTCH* signaling pathway-related genes, of which 67 genes were down-regulated and 23 genes were up-regulated (Fig. 5A-B). A cross-analysis between the differential genes of the *NOTCH* signaling pathway and the related genes of invasion and migration showed that 22 genes were down-regulated, and 3 genes were up-regulated under the influence of BPNS (Fig. 5C). As previous study proposed that the *WNT/β-catenin* regulates the Notch activity by modulating the expression of Notch ligand genes[41,42], we speculated that the inhibition of *WNT/β-catenin* signaling induced by BPNS may lead to Notch1 downregulation and further suppress the activation of the *NOTCH* signaling pathway. Interestingly, protein–protein interaction network showed *Notch1* was the hub gene between *WNT/β-catenin* and *NOTCH* signaling pathway (Fig. 5D).

To verify this conjecture, we tested the transcription and translation of key genes in the *NOTCH* signaling pathway, such as *Notch1*, *Jag1*, *Hes1*, *Cyc D3*, and *Akt1*. As shown in Fig. 5E-F, the related mRNA and corresponding proteins' expression of *NOTCH* signaling pathway in BPNS group were down-regulated. Consistently, the immunofluorescence results showed that Notch1 was significantly downregulated in the BPNS group compared to the blank control group (Fig. 5G-H). These results indicated that BPNS could inhibit the activation of Notch1-mediated *NOTCH* signaling pathway.

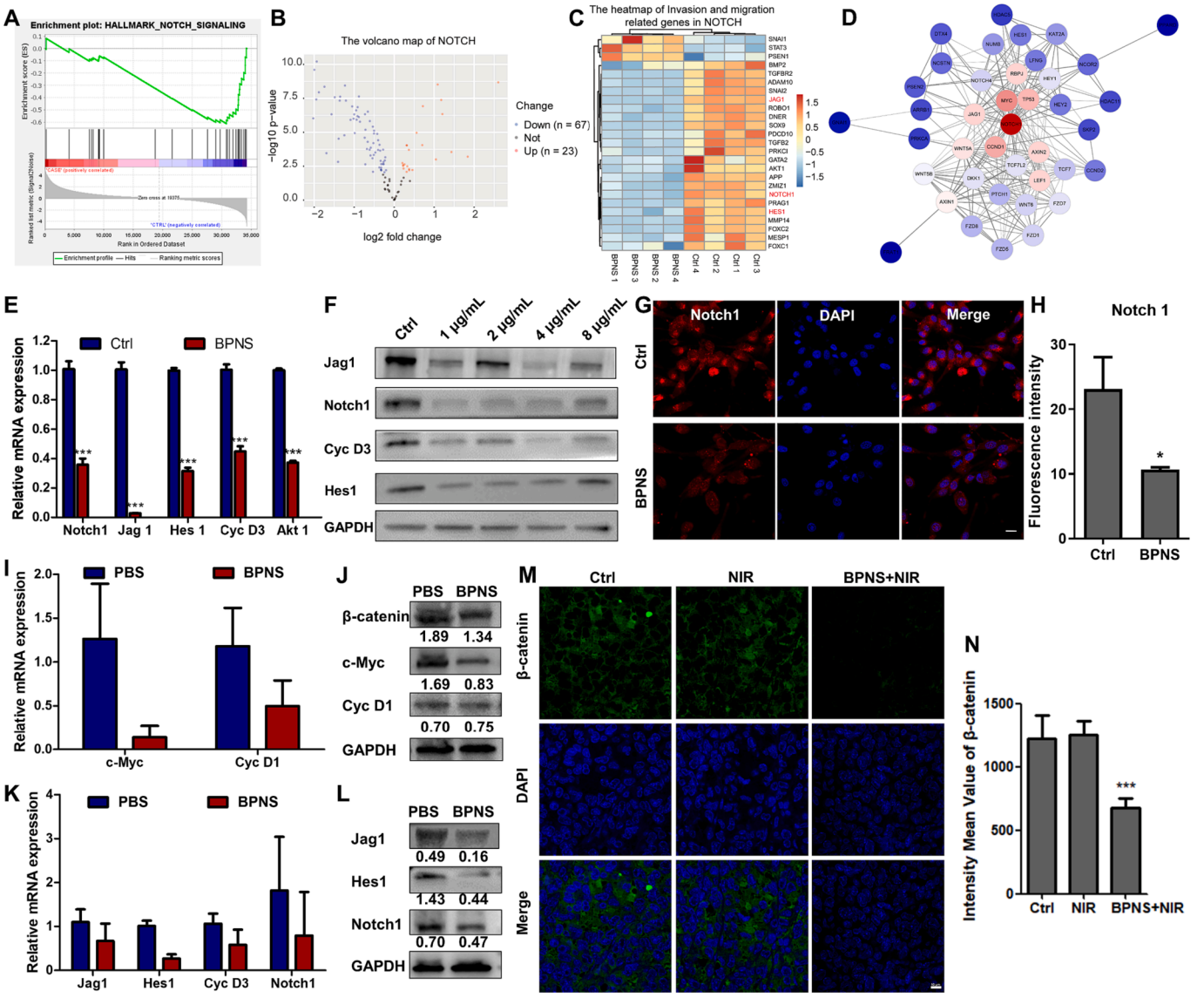

Fig. 5. BPNS inhibited the invasion and migration of GBM by suppressing the Notch1-mediated *NOTCH* signaling pathway. (A) GSEA plot of the *NOTCH* signaling pathway. (B) The volcano map of the gene in the *NOTCH* signaling pathway. (C) A cross-analysis between the differential gene of *NOTCH* signaling pathway and invasion and migration-related genes. (D) Protein-protein interaction network of *WNT/β-catenin* and *NOTCH* signaling pathway. (E) The qRT-PCR results of *Notch1*, *Jag1*, *Hes1*, *Cyc D3*, and *Akt1* of U87-MG cells after being treated with BPNS for 24 h. (F) The Western blot results of Notch1, Jag1, Hes1, Cyc D3 of U87-MG cells after being treated with BPNS (0, 1, 2, 4, 8 μg/mL) for 24 h. (G-H) The confocal image and the quantitative statistics of immunofluorescence of U87-MG cells after being treated with BPNS for 24 h, scale bar: 20 μm. (I) The qRT-PCR results of *c-Myc* and *cyc-D1* genes in *WNT/β-catenin* signaling pathway from subcutaneous tumor tissue. (J) The Western blot results of β-catenin, c-Myc and Cyc D1 from subcutaneous tumor tissue. (K) The qRT-PCR results of *Jag1*, *Hes1*, *Cyc D3*, and *Notch1* genes in *NOTCH* signaling pathway from subcutaneous tumor tissue. (L) The Western blot results of Jag1, Hes1, and Notch1 from subcutaneous tumor tissue. (M) Immunofluorescence staining results of β-catenin in orthotopic tumor tissue sections. (N) The quantification immunofluorescence staining results of β-catenin in brain tissue. Scale bar: 10 μm. Error bar, mean ± SD, $^{*}P < 0.05$, $^{***}P < 0.001$.

Further, we detected the expression of *WNT/β-catenin* and *NOTCH* signaling pathway-related molecules in tissues dissected from subcutaneous tumor. The qRT-PCR and Western blotting results showed BPNS downregulated the expression of β-catenin, Notch1, Jag1, and Hes1 *in vivo* (Fig. 5**I-L**). The results of immunofluorescence staining of orthotopic tumors showed that the expression of β-catenin was also significantly down-regulated after the treatment of BPNS (Fig. 5M-**N**). Immunohistochemical staining of CD31 in orthotopic tumor tissues showed that the BPNS treated group had clearer tumor boundaries and less angiogenesis when compared with control group (**Fig. S12**). These *in vivo* data further verified that BPNS inhibits the invasion and migration through the *WNT/β-catenin* and Notch1-mediated *NOTCH* signaling pathway activation, which was consistent with those of *in vitro* experiments.

3.6. BPNS directly bound to CSNK2A2, increasing GSK-3β activity, and inhibiting the WNT/β-catenin signaling pathway

Currently, we only know that BPNS inhibits the *WNT/β-catenin* signaling pathway, but how it works still needs further study. After analyzing the gene expression of *GSK-3β* and *β-catenin*, we found that the transcription of these two genes was not significantly affected by BPNS through RNA sequencing and qRT-PCR (Fig. 6A **and Fig. S13**). Additionally, we observed the protein expression of GSK-3β were not impacted by BPNS (Fig. 6A-B), but the protein level of β-catenin significantly decreased (Fig. 4I). GSK-3β is a multifunctional serine/threonine kinase playing a crucial role in protein phosphorylation, specifically increasing the phosphorylation level of β-catenin at the Ser 33 site[43]. This, in turn, promotes the degradation of β-catenin in the

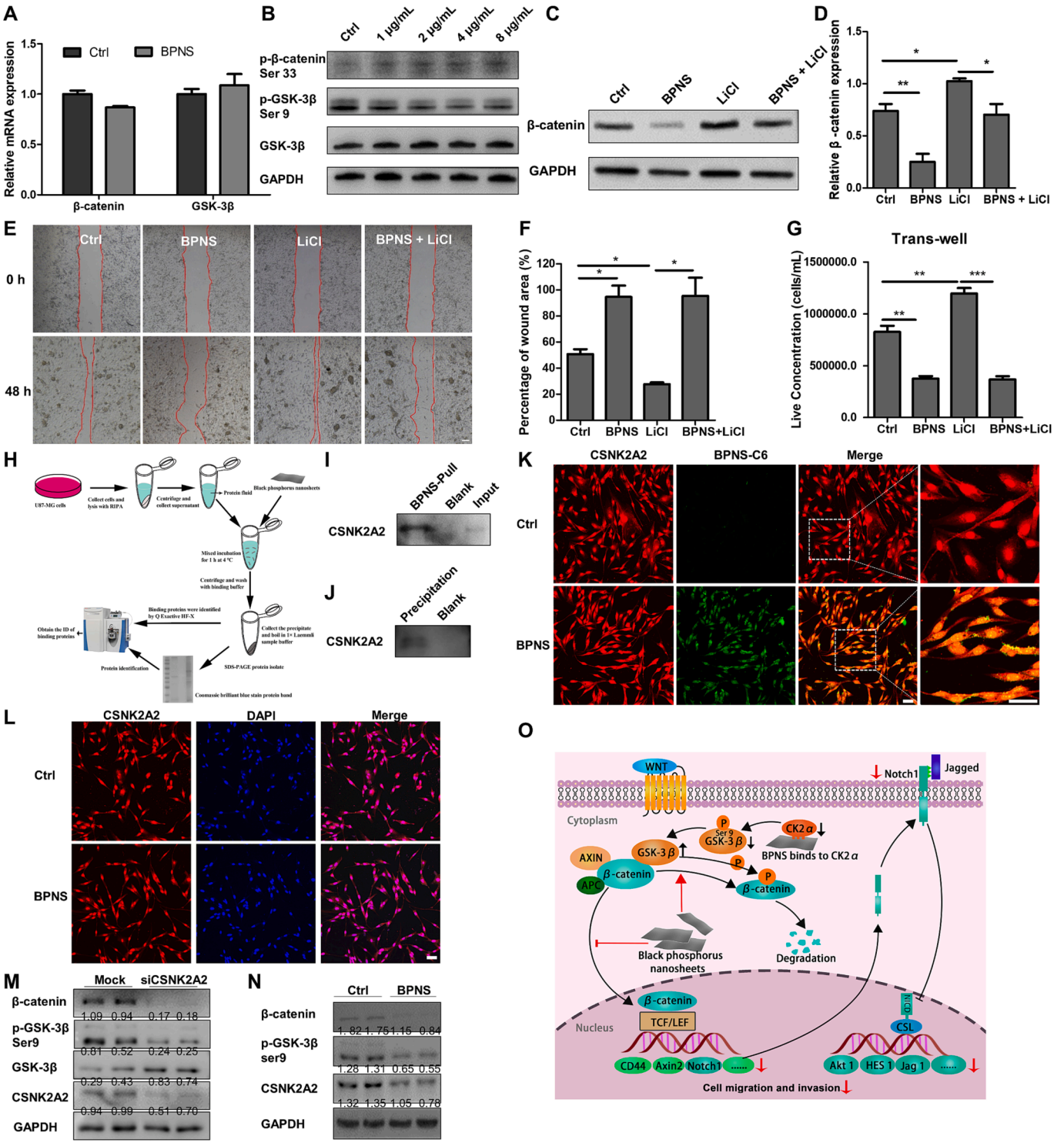

Fig. 6. The underlying mechanism by which BPNS inhibits the invasion and migration of glioblastoma cells was investigated. (A) The mRNA level of GSK-3β and β-catenin between control and BPNS group of U87-MG cells by qRT-PCR assay. (B) The Western blotting results of p-β-catenin Ser33, p-GSK-3β Ser9, GSK-3β, and GAPDH. (C) The Western blotting results of β-catenin expression after different treatments (the untreated group was used as the control group, BPNS group, 20 mM LiCl group, the BPNS combinate LiCl group) of the U87-MG cells. (D) The quantified Western blot experiment results of the relative β-catenin expression after different treatments ($n = 3$). (E) The wound healing results of U87-MG cells after different treatment for 48 h, scale bar: 200 μm. (F-G) The quantified wound area statistic assay and *trans*-well statistic assay results of U87-MG cells after different treatments for 48 h ($n = 3$). (H) The process diagram of protein identification, which is bound to the surface of BPNS, by LC-MS/MS. (I) The Western blot experiment confirmed that after co-incubation of BPNS with U87-MG cell proteins, BPNS can bind with the CSNK2A2 kinase. (J) The Western blot experiment results confirmed that BPNS which reacquired from the U87-MG cell lysates after BPNS treatment for 24 h, was bound with CSNK2A2 kinase. (K) The co-localization results of BPNS-C6 and CSNK2A2, scale bar: 50 μm. (L) The immunofluorescence image of CSNK2A2 after the treatment of BPNS for 24 h, scale bar: 50 μm. (M) The Western blotting results of β-catenin, p-GSK-3β Ser9, GSK-3β, and CSNK2A2 after knockdown of CSNK2A2 using siCSNK2A2. (N) The Western blotting results of β-catenin, p-GSK-3β Ser9, and CSNK2A2 after BPNS treatment for 24 h. (O) The mechanism diagram of BPNS inhibiting invasion and migration via *WNT/β-catenin* signaling pathway and Notch1-mediated *NOTCH* signaling pathway in the glioblastoma cell. Error bar, mean ± SD, $^{*}P < 0.05$, $^{**}P < 0.01$, $^{***}P < 0.001$.

cytoplasm. Consequently, the Western blot experiment results showed that after BPNS treatment, the phosphorylation level of GSK-3β at Ser9 was decreased, and the phosphorylation level of β-catenin at Ser33 was increased (Fig. 6B). This indicated that BPNS was likely to inhibit the *WNT/β-catenin* signaling pathway by increasing the activity of GSK-3β. To confirm this point, a GSK-3β active inhibitor LiCl was used to inhibit the activity of GSK-3β[44–46]. As shown in Fig. 6C-D, LiCl significantly upregulated the expression of β-catenin, whereas BPNS downregulated β-catenin level in the presence of LiCl. This suggested that the GSK-3β activity inhibited by LiCl was reactivated under the action of BPNS. Consistently, the wound-healing and *trans*-well experiments further confirmed BPNS suppressed the pro-migration and invasion effects of LiCl (Fig. 6**E-G**). Additionally, we investigated the impact of *WNT/β-catenin* signaling pathway activation on the *NOTCH* signaling pathway by adding LiCl. From the Western blot experiment results, we observed that the activation of the *WNT/β-catenin* pathway resulted in increased expression of Notch1 and its downstream protein HES1 whereas the addition of BPNS reversed this effect. These findings provided further evidence that BPNS inhibits the invasion and migration of malignant glioblastoma by targeting both the *WNT/β-catenin* signaling pathway and the Notch1-mediated *NOTCH* signaling pathway (**Fig. S14**).

The mechanism by which BPNS enhances the activity of GSK-3β remains unclear. To address this issue, we co-incubated BPNS with the whole-cell protein of U87-MG cells. After washing away proteins that did not bind to BPNS with washing buffer, the obtained BPNS-bound proteins were prepared into a protein solution, and protein mass spectrometry analysis was conducted using LC-MS/MS (Fig. 6H). From the protein identification data, we discovered that one of the proteins bound to BPNS is CSNK2A2 (CK2α), which has been reported to have phosphorylated and regulated the activity of GSK-3β [47,48]. Specifically, CSNK2A2 can phosphorylate GSK-3β at Ser9 and lead to the inhibition of GSK-3β activity[49]. Therefore, we speculated that CSNK2A2 may be the key target that BPNS regulates the activity of GSK-3β. Next, we generated protein complexes by co-incubating BPNS with the whole-cell protein and verified the interaction between BPNS and the protein kinase CSNK2A2 using immunoblotting (Fig. 6I). In a separate experiment, we treated U87-MG cells with BPNS for 24 h and collected the whole cell lysate to isolate the intracellular BPNS complexes. Similarly, we confirmed the intracellular binding of BPNS and CSNK2A2 using immunoblotting (Fig. 6J). Additionally, co-localization experiments of CSNK2A2 and BPNS further supported their interaction (Fig. 6K). In the results of the colocalization analysis in **Fig. S15**, we could observe the binding of BPNS to CSNK2A2 from the locations marked with arrows. Next, we detected the expression of CSNK2A2 after BPNS treatment. As shown in **Fig. S16**, the gene transcription level of *CSNK2A2* was not decreased by BPNS. The immunofluorescence results also showed that BPNS did not affected the expression of CSNK2A2 (Fig. 6L). The decreased CSNK2A2 protein detected in U87-MG cells were likely due to the binding of BPNS to intracellular CSNK2A2, which was subsequently removed during the cell lysis process through centrifugation. Based on the above results, we speculated that the binding of BPNS to CSNK2A2 protein would not degrade it but reduce its kinase activity, leading to a decrease in the phosphorylation level of GSK-3β and an increase in its activity. To validate this, we detected the phosphorylation level of GSK-3β at ser9 and it was significantly decreased after treated by BPNS (Fig. 6N). Additionally, we transfected siCSNK2A2 to inhibit the translation of CSNK2A2. From the Western blot experiment results, it can be observed that we successfully suppressed the expression of CSNK2A2 kinase (Fig. 6M). Subsequent Western blot data also confirmed that the silencing of CSNK2A2 reduced the phosphorylation level of GSK-3β and increased the kinase activity of GSK-3β, resulting in a decrease in the protein level of β-catenin (Fig. 6**M**). The protein expression levels of U87-MG cells after CSNK2A2 gene silencing were similar to the protein expression inhibition observed after BPNS treatment (Fig. 6N). This similarity indicated that the binding of BPNS to CSNK2A2 led to a decrease in its kinase activity, thereby reducing the phosphorylation of GSK-3β at the Ser9, resulting in increased activity of GSK-3β and then enhanced degradation of β-catenin. In summary, our study demonstrated that BPNS can activate the activity of GSK-3β by binding to CSKN2A2, leading to the degradation of β-catenin, thereby inactivating the *WNT/β-catenin* and *NOTCH* pathways, and finally inhibiting the invasion and development of glioblastoma cells (Fig. 6O).

4. Discussion

The present study provides new insights into the potential of BPNS in inhibiting the invasion and migration of glioblastoma cells. The findings demonstrate that BPNS acts by inhibiting the *WNT/β-catenin* and *NOTCH* signaling pathways, which are crucial in regulating tumor progression. This inhibition results from the interaction of BPNS with CSNK2A2, leading to reduced phosphorylation of GSK-3β at Ser9. As a result of this inhibition, GSK-3β promotes the degradation of β-catenin at Ser 33, preventing its transportation into the nucleus. Consequently, downstream genes of the *WNT/β-catenin* pathway, such as Axin2, CD44, and Notch1, are inhibited. Furthermore, the reduction of Notch1 leads to the downregulation of Jag1, Hes1, and Akt1, effectively inhibiting the *NOTCH* pathway. The combined suppression of both *WNT/β-catenin* and *NOTCH* pathways results in the inhibition of glioblastoma cell migration and invasion. Based on its role in inhibiting these two signaling pathways, BPNS may also provide new therapeutic approaches for other highly invasive and migratory tumors in future research.

It is important to note that glioblastoma patients often face challenges in therapy due to the high rates of migration and invasion of tumor cells. While BPNS-based nanomedicines may not entirely eliminate tumor cells, they demonstrate significant efficacy in inhibiting their proliferation, migration, and invasion. This suggests that BPNS could be a promising candidate for combination therapy for GBM.

Based on the unique anti-tumor capabilities of BPNS, subsequent research can progress towards the development of nano drugs based on BPNS. The physicochemical properties of BPNS allow for targeted modifications on its surface, incorporating targeted peptides or molecules with the ability to penetrate the blood–brain barrier (BBB) or further target tumor tissues, enhancing its capacity to cross the BBB. Furthermore, after targeted modifications, we can leverage BPNS to load chemotherapy drugs or gene therapy drugs, achieving a combined treatment for gliomas or other tumors. Additionally, BPNS can be prepared as a drug-loaded sustained-release formulation, placed at the lesion site for postoperative treatment of gliomas, preventing the invasion of glioma cells and the recurrence of tumors near the resected area.

While the study provides significant insights into the cellular mechanisms of BPNS on tumor cells, it acknowledges that further research is needed to fully understand BPNS's effects in treating glioblastoma. We can also broaden our perspective, starting from the mechanism of BPNS binding to intracellular proteins CSNK2A2 and inhibiting the invasion and migration of glioblastoma cells. We can explore whether BPNS can bind to other intracellular proteins and delve into the profound investigation of the impact of such protein binding on the biological activity of tumor cells.

Overall, the key findings and implications of this study emphasize the potential of BPNS-based nanomedicine as a promising therapeutic option for glioblastoma treatment. It also highlights avenues for future research to unlock the full potential of BPNS in combatting this aggressive form of brain cancer.

CRediT authorship contribution statement

Yue Xiong: Conceptualization, Data curation, Formal analysis, Investigation, Methodology, Project administration, Software, Validation, Visualization, Writing – original draft, Writing – review & editing. **Chao He:** Data curation, Methodology, Software, Writing – original draft, Writing – review & editing. **Xun Lin:** Formal analysis, Methodology, Resources, Visualization. **Ke Cheng:** Formal analysis,

Methodology, Writing – original draft. **Fumei He:** Formal analysis, Methodology, Software. **Jingxin Zhao:** Methodology, Validation. **Mengjie Yang:** Investigation, Resources. **Hong Gao:** Methodology, Visualization. **Fangjie He:** Investigation, Resources. **Xiaopei Zhang:** Writing – original draft. **Zeqi Liu:** Methodology. **Gan Liu:** Conceptualization, Supervision, Writing – original draft. **Wenbin Deng:** Conceptualization, Funding acquisition, Project administration, Supervision, Writing – original draft, Writing – review & editing.

Declaration of competing interest

The authors declare that they have no known competing financial interests or personal relationships that could have appeared to influence the work reported in this paper.

Data availability

Data will be made available on request.

Acknowledgements

The authors acknowledge the funding support from Shenzhen Science and Technology Program (Grant No. KQTD20190929173853397, China), National Natural Science Foundation of China (Grant No. 81971081, China), the Innovation and Technology Fund of Guangzhou (201803010090, China).

Appendix A. Supplementary data

Supplementary data to this article can be found online at https://doi.org/10.1016/j.cej.2024.148614.

References

[1] H. Huang, B. Jiang, X.M. Zou, X.Z. Zhao, L. Liao, Black phosphorus electronics, Sci. Bull. 64 (15) (2019) 1067–1079, https://doi.org/10.1016/j.scib.2019.02.015.
[2] R. Gusmão, Z. Sofer, M. Pumera, Black phosphorus rediscovered: from bulk material to monolayers, Angew. Chem. Int. Ed. Engl. 56 (28) (2017) 8052–8072, https://doi.org/10.1002/anie.201610512.
[3] J. Ding, G. Qu, P.K. Chu, X.-F. Yu, Black phosphorus: Versatile two-dimensional materials in cancer therapies, View 2 (1) (2021), https://doi.org/10.1002/viw.20200043.
[4] J.D. Shao, H.H. Xie, H. Huang, Z.B. Li, Z.B. Sun, Y.H. Xu, Q.L. Xiao, X.F. Yu, Y. T. Zhao, H. Zhang, H.Y. Wang, P.K. Chu, Biodegradable black phosphorus-based nanospheres for in vivo photothermal cancer therapy, Nat Commun 7 (2016), https://doi.org/10.1038/ncomms12967.
[5] J.R. Choi, K.W. Yong, J.Y. Choi, A. Nilghaz, Y. Lin, J. Xu, X. Lu, Black Phosphorus and its Biomedical Applications, Theranostics 8 (4) (2018) 1005–1026, https://doi.org/10.7150/thno.22573.
[6] M. Ou, C. Lin, Y. Wang, Y. Lu, W. Wang, Z. Li, W. Zeng, X. Zeng, X. Ji, L. Mei, Heterojunction engineered bioactive chlorella for cascade promoted cancer therapy, J Control Release 345 (2022) 755–769, https://doi.org/10.1016/j.jconrel.2022.03.059.
[7] F.C. Zeng, H. Qin, L.M. Liu, H.C. Chang, Q. Chen, L.H. Wu, L. Zhang, Z.J. Wu, D. Xing, Photoacoustic-immune therapy with a multi-purpose black phosphorus-based nanoparticle, Nano Res 13 (12) (2020) 3403–3415, https://doi.org/10.1007/s12274-020-3028-x.
[8] W. Liu, A. Dong, B. Wang, H. Zhang, Current advances in black phosphorus-based drug delivery systems for cancer therapy, Adv Sci 8 (5) (2021), https://doi.org/10.1002/advs.202003033.
[9] Y.F. Xu, F. Ren, H.H. Liu, H. Zhang, Y.B. Han, Z. Liu, W.L. Wang, Q. Sun, C.J. Zhao, Z. Li, Cholesterol-modified black phosphorus nanospheres for the first NIR-II fluorescence bioimaging, ACS Appl Mater Interfaces 11 (24) (2019) 21399–21407, https://doi.org/10.1021/acsami.9b05825.
[10] W. Tao, X. Zhu, X. Yu, X. Zeng, Q. Xiao, X. Zhang, X. Ji, X. Wang, J. Shi, H. Zhang, L. Mei, Black phosphorus nanosheets as a robust delivery platform for cancer theranostics, Adv. Mater. 29 (1) (2017), https://doi.org/10.1002/adma.201603276.
[11] R.J. Gui, H. Jin, Z.H. Wang, J.H. Li, Black phosphorus quantum dots: synthesis, properties, functionalized modification and applications, Chem. Soc. Rev. 47 (17) (2018) 6795–6823, https://doi.org/10.1039/c8cs00387d.
[12] W.Q. Ou, J.H. Byeon, R.K. Thapa, S.K. Ku, C.S. Yong, J.O. Kim, Plug-and-play nanorization of coarse black phosphorus for targeted chemo-photoimmunotherapy of colorectal cancer, Acs Nano 12 (10) (2018) 10061–10074, https://doi.org/10.1021/acsnano.8b04658.
[13] H. Qin, J. Chen, Y. Li, L. Gao, J. Wang, G. Qu, M. Yang, X. Zhou, Z. Sun, Inflammatory response induced by black phosphorus nanosheets in mice and macrophages, Sci. Total Environ. 782 (2021), https://doi.org/10.1016/j.scitotenv.2021.146860.
[14] W. Zhou, T. Pan, H. Cui, Z. Zhao, P.K. Chu, X.-F. Yu, Black phosphorus: bioactive nanomaterials with inherent and selective chemotherapeutic effects, Angew. Chem. Int. Ed. 58 (3) (2019) 769–774, https://doi.org/10.1002/anie.201810878.
[15] G. Qu, T. Xia, W. Zhou, X. Zhang, H. Zhang, L. Hu, J. Shi, X.F. Yu, G. Jiang, Property-activity relationship of black phosphorus at the nano-bio interface: from molecules to organisms, Chem. Rev. 120 (4) (2020) 2288–2346, https://doi.org/10.1021/acs.chemrev.9b00445.
[16] X. Shao, Z. Ding, W. Zhou, Y. Li, Z. Li, H. Cui, X. Lin, G. Cao, B. Cheng, H. Sun, M. Li, K. Liu, D. Lu, S. Geng, W. Shi, G. Zhang, Q. Song, L. Chen, G. Wang, W. Su, L. Cai, L. Fang, D.T. Leong, Y. Li, X.-F. Yu, H. Li, Intrinsic bioactivity of black phosphorus nanomaterials on mitotic centrosome destabilization through suppression of PLK1 kinase, Nat. Nanotechnol. 16 (10) (2021) 1150-+, https://doi.org/10.1038/s41565-021-00952-x.
[17] B.M. Alexander, T.F. Cloughesy, A. Glioblastoma, J. Clin. Oncol. 35 (21) (2017) 2402-+, https://doi.org/10.1200/jco.2017.73.0119.
[18] D.P. Sun, Y.W. Lee, J.T. Chen, Y.W. Lin, R.M. Chen, The Bradykinin-BDKRB1 Axis Regulates Aquaporin 4 Gene Expression and Consequential Migration and Invasion of Malignant Glioblastoma Cells via a Ca2+-MEK1-ERK1/2-NF-kappa B Mechanism, Cancers 12 (3) (2020), https://doi.org/10.3390/cancers12030667.
[19] X.P. Zhou, Z. Liu, Q. Shi, J.T. Jiao, W.B. Bian, X. Song, J.B. Mo, B. Sang, Y.F. Xu, J. M. Qian, Y.W. Chao, R.T. Yu, Geranylgeranyltransferase I regulates HIF-1 alpha promoting glioblastoma cell migration and invasion, J. Neuro-Oncol. 112 (3) (2013) 365–374, https://doi.org/10.1007/s11060-013-1081-y.
[20] S.Y. Lee, Temozolomide resistance in glioblastoma multiforme, Genes Dis. 3 (3) (2016) 198–210, https://doi.org/10.1016/j.gendis.2016.04.007.
[21] W. Chen, J. Ouyang, X. Yi, Y. Xu, C. Niu, W. Zhang, L. Wang, J. Sheng, L. Deng, Y.-N. Liu, S. Guo, Black Phosphorus Nanosheets as a Neuroprotective Nanomedicine for Neurodegenerative Disorder Therapy, Adv. Mater. 30 (3) (2018), https://doi.org/10.1002/adma.201703458.
[22] S. Xiong, Z. Li, Y. Liu, Q. Wang, J. Luo, X. Chen, Z. Xie, Y. Zhang, H. Zhang, T. Chen, Brain-targeted delivery shuttled by black phosphorus nanostructure to treat Parkinson's disease, Biomaterials 260 (2020), https://doi.org/10.1016/j.biomaterials.2020.120339.
[23] L.G. Jin, P. Hu, Y.Y. Wang, L.J. Wu, K. Qin, H.X. Cheng, S.H. Wang, B.X. Pan, H. B. Xin, W.H. Zhang, X.L. Wang, Fast-Acting Black-Phosphorus-Assisted Depression Therapy with Low Toxicity, Adv. Mater. 32 (2) (2020), https://doi.org/10.1002/adma.201906050.
[24] X. Huang, K. Ren, Z. Chang, Y. Ye, D. Huang, W. Zhao, L. Yang, Y. Dong, Z. Cao, H. Qiao, Glucose oxidase and L-arginine functionalized black phosphorus nanosheets for multimodal targeted therapy of glioblastoma, Chem. Eng. J. 430 (2022) 132898, https://doi.org/10.1016/j.cej.2021.132898.
[25] J. Qi, Y. Xiong, K. Cheng, Q. Huang, J. Cao, F. He, L. Mei, G. Liu, W. Deng, Heterobifunctional PEG-grafted black phosphorus quantum dots: "Three-in-One" nano-platforms for mitochondria-targeted photothermal cancer therapy, Asian J Pharm Sci 16 (2) (2021) 222–235, https://doi.org/10.1016/j.ajps.2020.09.001.
[26] Y. Li, Z. Du, X.P. Liu, M.M. Ma, D.Q. Yu, Y. Lu, J.S. Ren, X.G. Qu, Near-infrared activated black phosphorus as a nontoxic photo-oxidant for Alzheimer's amyloid-beta peptide, Small 15 (24) (2019), https://doi.org/10.1002/smll.201901116.
[27] Z. Li, C. Zhao, Q. Fu, J. Ye, L. Su, X. Ge, L. Chen, J. Song, H. Yang, Neodymium (3+)-coordinated black phosphorus quantum dots with retrievable NIR/X-ray optoelectronic switching effect for anti-glioblastoma, Small (2021), https://doi.org/10.1002/smll.202105160.
[28] M. Vinci, C. Box, S.A. Eccles, Three-Dimensional (3D) tumor spheroid invasion assay, JOVE-J. Vis. Exp. 99 (2015), https://doi.org/10.3791/52686.
[29] Z. Chai, D. Ran, L. Lu, C. Zhan, H. Ruan, X. Hu, C. Xie, K. Jiang, J. Li, J. Zhou, J. Wang, Y. Zhang, R.H. Fang, L. Zhang, W. Lu, Ligand-modified cell membrane enables the targeted delivery of drug nanocrystals to glioma, ACS Nano 13 (5) (2019) 5591–5601, https://doi.org/10.1021/acsnano.9b00661.
[30] J. Wang, Y. Zou, X.C. Wu, M. Chen, S. Zhang, X.J. Lu, Q. Wang, DACH1 inhibits glioma invasion and tumor growth via the Wnt/catenin pathway, OncoTargets Ther. 11 (2018) 5853–5863, https://doi.org/10.2147/ott.s168314.
[31] L. He, H. Zhou, Z.Q. Zeng, H.L. Yao, W.P. Jiang, H.T. Qu, Wnt/beta-catenin signaling cascade: A promising target for glioma therapy, J. Cell. Physiol. 234 (3) (2019) 2217–2228, https://doi.org/10.1002/jcp.27186.
[32] B. Wallmen, M. Schrempp, A. Hecht, Intrinsic properties of Tcf1 and Tcf4 splice variants determine cell-type-specific Wnt/β-catenin target gene expression, Nucleic Acids Res. 40 (19) (2012) 9455–9469, https://doi.org/10.1093/nar/gks690.
[33] X. Ji, H. Guo, S. Yin, H. Du, miR-139-5p functions as a tumor suppressor in cervical cancer by targeting TCF4 and inhibiting Wnt/β-catenin signaling, Onco Targets Ther. 12 (2019) 7739–7748, https://doi.org/10.2147/ott.s215796.
[34] H. Xu, M. Niu, X. Yuan, K. Wu, A. Liu, CD44 as a tumor biomarker and therapeutic target, EXP HEMATOL ONCOL 9 (1) (2020), https://doi.org/10.1186/s40164-020-00192-0.
[35] G. Safarians, A. Sohrabi, I. Solomon, W. Xiao, S. Bastola, B.W. Rajput, M. Epperson, I. Rosenzweig, K. Tamura, B. Singer, J. Huang, M.J. Harrison, T. Sanazzaro, M. C. Condro, H.I. Kornblum, S.K. Seidlits, Glioblastoma spheroid invasion through soft, brain-like matrices depends on hyaluronic acid-CD44 interactions, Adv. Healthc. Mater. 12 (14) (2023), https://doi.org/10.1002/adhm.202203143.
[36] F. Wei, Q. Wang, Q. Su, H. Huang, J. Luan, X. Xu, J. Wang, miR-373 inhibits glioma cell U251 migration and invasion by down-regulating CD44 and TGFBR2, Cell. Mol. Neurobiol. 36 (8) (2016) 1389–1397, https://doi.org/10.1007/s10571-016-0338-3.

[37] S. Feng, K. Wang, Z. Shao, Q. Lin, B. Li, P. Liu, MiR-373/miR-520s-CD44 axis significantly inhibits the growth and invasion of human glioblastoma cells, Archives of Medical Research 53 (6) (2022) 550–561, https://doi.org/10.1016/j.arcmed.2022.08.003.

[38] D. Maciaczyk, D. Picard, L. Zhao, K. Koch, D. Herrera-Rios, G. Li, V. Marquardt, D. Pauck, T. Hoerbelt, W. Zhang, D.M. Ouwens, M. Remke, T. Jiang, H.J. Steiger, J. Maciaczyk, U.D. Kahlert, CBF1 is clinically prognostic and serves as a target to block cellular invasion and chemoresistance of EMT-like glioblastoma cells, Br. J. Cancer 117 (1) (2017) 102–112, https://doi.org/10.1038/bjc.2017.157.

[39] L. Yi, X. Zhou, T. Li, P. Liu, L. Hai, L. Tong, H. Ma, Z. Tao, Y. Xie, C. Zhang, S. Yu, X. Yang, Notch1 signaling pathway promotes invasion, self-renewal and growth of glioma initiating cells via modulating chemokine system CXCL12/CXCR4, J. Experiment. Clin. Cancer Res. CR 38 (1) (2019) 339, https://doi.org/10.1186/s13046-019-1319-4.

[40] H. Raghu, C.S. Gondi, D.H. Dinh, M. Gujrati, J.S. Rao, Specific knockdown of uPA/uPAR attenuates invasion in glioblastoma cells and xenografts by inhibition of cleavage and trafficking of Notch -1 receptor, Mol Cancer 10 (2011) 130, https://doi.org/10.1186/1476-4598-10-130.

[41] N. Krishnamurthy, R. Kurzrock, Targeting the Wnt/beta-catenin pathway in cancer: Update on effectors and inhibitors, Cancer Treat. Rev. 62 (2018) 50–60, https://doi.org/10.1016/j.ctrv.2017.11.002.

[42] J. So, M. Khaliq, K. Evason, N. Ninov, B.L. Martin, D.Y.R. Stainier, D. Shin, Wnt/β-catenin signaling controls intrahepatic biliary network formation in zebrafish by regulating notch activity, Hepatology 67 (6) (2018) 2352–2366, https://doi.org/10.1002/hep.29752.

[43] C.M. Liu, Y.M. Li, M. Semenov, C. Han, G.H. Baeg, Y. Tan, Z.H. Zhang, X.H. Lin, X. He, Control of beta-catenin phosphorylation/degradation by a dual-kinase mechanism, Cell 108 (6) (2002) 837–847, https://doi.org/10.1016/s0092-8674(02)00685-2.

[44] M.Y. Xia, X.Y. Zhao, Q.L. Huang, H.Y. Sun, C. Sun, J. Yuan, C. He, Y. Sun, X. Huang, W. Kong, W.J. Kong, Activation of Wnt/β-catenin signaling by lithium chloride attenuates d-galactose-induced neurodegeneration in the auditory cortex of a rat model of aging, FEBS Open Bio 7 (6) (2017) 759–776, https://doi.org/10.1002/2211-5463.12220.

[45] L. Bai, H.-M. Chang, J.-C. Cheng, G. Chu, P.C.K. Leung, G. Yang, Lithium chloride inhibits StAR and progesterone production through GSK-3 beta and ERK1/2 signaling pathways in human granulosa-lutein cells, Mol. Cell. Endocrinol. 461 (C) (2018) 89–99, https://doi.org/10.1016/j.mce.2017.08.018.

[46] T. Shan, C. Zhou, R. Yang, F. Yan, P. Zhang, Y. Fu, H. Jiang, Lithium chloride promotes the odontoblast differentiation of hair follicle neural crest cells by activating Wnt/β-catenin signaling, Cell Biol. Int. 39 (1) (2015) 35–43, https://doi.org/10.1002/cbin.10340.

[47] A. Wu, M. Li, Z. Mai, S. Li, Z. Yang, CK2α Regulates the Metastases and Migration of Lung Adenocarcinoma A549 Cell Line through PI3K/Akt/GSK-3β Signal Pathway, Zhongguo Fei Ai Za Zhi 20 (4) (2017) 233–238, https://doi.org/10.3779/j.issn.1009-3419.2017.04.11.

[48] S.Y. Park, H.K. Shin, W.S. Lee, S.S. Bae, K. Kim, K.W. Hong, C.D. Kim, Neuroprotection by aripiprazole against β-amyloid-induced toxicity by P-CK2α activation via inhibition of GSK-3β, Oncotarget 8 (66) (2017) 110380–110391, https://doi.org/10.18632/oncotarget.22777.

[49] Y.J. Wang, Z.D. Lv, F.H. Chen, X. Wang, S.H. Gou, Discovery of 5-(3-chlorophenylamino)benzo c 2,6 naphthyridine derivatives as highly selective CK2 inhibitors with potent cancer cell stemness inhibition, j. Med. Chem. 64 (8) (2021) 5082–5098, https://doi.org/10.1021/acs.jmedchem.1c00131.